Combined Ab Initio Computational and Solid-State ^{17}O MAS NMR Studies of Crystalline P_2O_5

Brian R. Cherry,*,† Todd M. Alam,† Carol Click,‡,§ Richard K. Brow,‡ and Zhehong Gan||

Sandia National Laboratories, Department of Organic Materials, Albuquerque, New Mexico 87185-0888, University of Missouri−Rolla, Ceramic Engineering Department, Rolla, Missouri 65409-0330, and National High Magnetic Field Laboratory, Tallahassee, Florida 32310

Received: October 21, 2002; In Final Form: January 22, 2003

Ab initio calculations of the ^{17}O electrical field gradient (EFG) tensor quadrupolar coupling constant (C_Q) and asymmetry parameter (η_Q), along with the ^{17}O NMR isotropic chemical shift (δ_{iso}) for the three crystalline polymorphs of P_2O_5 are presented. These computational results are compared with experimental values for crystalline *h*-P_2O_5 (hexagonal-form) obtained using a combination of solid-state ^{17}O magic angle spinning (MAS) NMR at three different magnetic field strengths (9.4, 14.1, and 19.6 T), two-dimensional (2D) multiple-quantum (MQ)MAS NMR, and 2D satellite-transition (ST)MAS NMR experiments. In addition ab initio studies of the model $H_4P_2O_7$ cluster allowed empirical correlations between the bridging oxygen EFG parameters and the P−O−P bond angle to be developed.

Introduction

The use of solid-state ^{17}O nuclear magnetic resonance (NMR) spectroscopy to study amorphous and disordered materials is on the rise due to the strong correlations between the local structural environment of the oxygen and the ^{17}O NMR parameters. The ability to correlate ^{17}O NMR parameters with specific structural factors including variations in bridging oxygen bond angle, oxygen bond lengths, effective charge, cation coordination, coordinating cation−oxygen distances, and coordinating cation electronegativity has become an important tool in the investigation of inorganic oxide networks. For example, the local environment of bridging oxygens in silicate systems has been extensively investigated with ^{17}O NMR.[1−9] From the early work by Tossell and co-workers,[10−12] to the more recent work by Grandinetti and co-workers,[1,13,14] ab initio computational studies have been used to predict and correlate the ^{17}O NMR quadrupolar parameters with local structure. In particular, the correlations between the Si−O−Si bond angle and the quadrupolar coupling constant (C_Q) or the quadrupolar asymmetry parameter (η_Q) of the ^{17}O electrical field gradient (EFG) tensor have been used as a probe of structure. These ab initio calculations of structural correlations have recently been extended to basic X−O−X systems (where X = B, C, Al, Si, Ga, Ge, P, and As).[14]

Computational and experimental investigations of correlations between ^{17}O NMR parameters and structural components in phosphate systems have received much less attention. Only a limited number of model compounds in the phosphate system appear in the literature.[15−19] Ab initio computations of ^{17}O quadrupole parameters of phosphate systems have also been undertaken to a varying degree of success.[12,14] One of the major reasons for the lack of ^{17}O investigations in phosphate systems is that the phosphorus hybridization allows for the presence of double-bonded terminal oxygens (TO, P═O) in addition to the more standard bridging oxygen (BO, P−O−P) and nonbonding oxygen (NBO, P−O^-) environments. In addition, there are limited numbers of crystalline model compounds reported in the literature, especially in the ultraphosphate (O/P < 3) regime. Recently, the first studies utilizing solid-state ^{17}O NMR for phosphate glasses appeared in the literature,[20,21] leading the way for future investigations of amorphous phosphate systems.

In the work presented here, ab initio calculations of the ^{17}O NMR parameters for the three crystalline polymorphs of P_2O_5 are reported. These polymorphs include the metastable hexagonal form (*h*-P_2O_5)[22] and the two orthorhombic forms *o*-P_2O_5 and *o*′-P_2O_5.[23,24] To verify the accuracy of the ab initio calculations, the experimental solid-state ^{17}O NMR results for ^{17}O-labeled crystalline *h*-P_2O_5 are also presented. This study represents the first detailed experimental ^{17}O NMR study of the crystalline P_2O_5 system and a crystalline phosphate material containing bridging oxygens within a P−O−P motif. The variation of the ^{17}O EFG parameters with changes in the bridging P−O−P bond angle are derived by using the model cluster $H_4P_2O_7$. These studies allowed the development of empirical correlation between C_Q, η_Q, and the bridging P−O−P bond angle. These correlations, along with the results from the P_2O_5 polymorphs are compared and discussed.

Experimental Section

Theoretical Methods. The ab initio calculations were performed using GAUSSIAN 98[25] on either a SGI O2 workstation or an 8-node DEC Alpha workstation. All cluster geometry optimizations were performed using density functional theory (DFT) methods at the B3LYP/6-311++G(2p,2d) level of theory. B3LYP designates Becke's[26] three-parameter hybrid exchange functional along with the correlational functional of

* To whom correspondence should be addressed.
† Sandia National Laboratories.
‡ University of Missouri−Rolla.
§ Present address Schott Glass Technologies Inc., Duryea, PA 18642-2036.
|| National High Magnetic Field Laboratory.

10.1021/jp0272670 CCC: $25.00
Published on Web 05/02/2003

TABLE 1: Ab Initio Calculation of ^{17}O Chemical Shift and EFG Parameters for Crystalline Polymorphs of P_2O_5 and H_2O

		HF					B3LYP				
	θ^a (deg)	σ_{iso} (ppm)	δ_{iso} (ppm)	$C_Q{}^b$ (MHz)	$C_Q{}^c$ (MHz)	η_Q	σ_{iso} (ppm)	δ_{iso} (ppm)	$C_Q{}^b$ (MHz)	$C_Q{}^c$ (MHz)	η_Q
					h-$P_2O_5{}^d$						
TO(1)		220.7	99.0	−4.88	−4.36	0.00	187.5	131.2	−4.53	−4.19	0.00
TO(4)		221.1	98.6	−4.79	−4.28	0.02	187.8	130.9	−4.46	−4.12	0.02
BO(2)	122.6	201.0	118.7	−8.64	−7.71	0.63	163.6	155.1	−8.19	−7.57	0.61
BO(3)	123.0	202.4	117.3	−8.64	−7.71	0.61	165.1	153.6	−8.20	−7.58	0.59
					o-$P_2O_5{}^e$						
TO(1)^f		205.2	114.5	−4.81	−4.29	0.02	158.6	160.1	−4.55	−4.20	0.03
BO(1)^g	123.0	200.5	119.2	−9.04	−8.07	0.53	156.7	162.0	−8.79	−8.12	0.48
BO(2)	135.7	206.1	113.6	−9.48	−8.46	0.30	162.8	155.9	−9.15	−8.46	0.28
		216.1	103.6	−9.66	−8.62	0.27	179.5	139.2	−9.31	−8.60	0.24
					o′-$P_2O_5{}^e$						
TO(1a)^{f,h}		205.9	113.8	−5.07	−4.53	0.09	154.0	164.7	−4.78	−4.42	0.10
BO(1a)	143.7	215.2	104.5	−10.18	−9.09	0.19	172.2	146.5	−9.82	−9.08	0.17
BO(2a)	139.9	211.6	108.1	−9.87	−8.81	0.29	172.3	146.4	−9.57	−8.84	0.28
TO(1b)^{f,i}		211.7	108.0	−4.67	−4.17	0.16	171.0	147.7	−4.41	−4.08	0.16
BO(1b)	143.7	208.5	111.2	−9.74	−8.69	0.23	161.0	157.7	−9.30	−8.59	0.24
BO(2b)	139.9	208.5	111.2	−9.84	−8.78	0.28	168.6	150.1	−9.38	−8.67	0.28

	HF			B3LYP			experimental	
	σ_{iso} (ppm)	C_Q (MHz)	η_Q	σ_{iso} (ppm)	C_Q (MHz)	η	C_Q (MHz)	η_Q
$H_2O{}^j$	327.6	11.11	0.80	327.0	10.75	0.77	10.175 (67)	0.75 (1)
$H_2O{}^k$	319.7	11.40	0.78	318.7	11.01	0.75		

[a] Bridging P−O−P bond angle. [b] All calculation obtained using a 6-311++(2p,2d) basis set. Quadrupolar coupling (C_Q) obtained from Gaussian 98 program. [c] C_Q normalized to the H_2O molecule with experimentally determined equilibrium geometry. [d] NMR calculations performed on the P_4O_{10} primitive cell. Atom numbering corresponds to the numbering from the X-ray investigation. [e] NMR calculations performed on the H-terminated $H_6P_4O_{13}$ cluster created from the crystal structure. [f] Calculated values for only the central TO in the $H_6P_4O_{13}$ cluster are reported. [g] For the $H_6P_4O_{13}$ cluster there are two inequivalent BO. [h] Calculations based on the H-terminated $H_6P_4O_{13}$ cluster centered on the TO with a PO bond length of 1.4515 Å. [i] Calculations based on the H-terminated $H_6P_4O_{13}$ cluster centered on the TO with a PO bond length of 1.4372 Å. [j] Equilibrium geometry, corrected for vibration/rotation, R(O−H) = 0.957 Å. [k] Equilibrium geometry, R(O−H) = 0.972 Å.

Lee, Yang, and Parr.[27] The ^{17}O chemical shield anisotropy (CSA) and electrical field gradient (EFG) calculations were obtained using both the Hartree−Fock (HF) and the DFT B3LYP method along with a 6-311++G(2p,2d) basis set. The ^{17}O NMR chemical shielding calculations employed the gauge-including atomic orbital (GIAO) method.[28] The ^{17}O isotropic chemical shifts (δ_{iso}) were referenced to shielding of H_2O obtained at the same level of theory using

$$\delta_{iso}(\text{cluster}) = \sigma_{iso}(H_2O) - \sigma_{iso}(\text{cluster}) \quad (1)$$

where the isotropic shielding (σ_{iso}) is given by the trace of the CSA tensor in the principal axis system (PAS). The quadrupolar coupling constant (C_Q) and the asymmetry parameter (η_Q) of the traceless EFG tensor were obtained using

$$C_Q = e^2 q_{zz} Q/h \quad (2)$$

$$\eta_Q = \frac{eq_{xx} - eq_{yy}}{eq_{zz}} \quad (3)$$

where eQ is the nuclear quadrupolar moment of ^{17}O, and eq_{xx}, eq_{yy}, and eq_{zz} are the principal components of the EFG tensor defined by the relation $|eq_{zz}| \geq |eq_{yy}| \geq |eq_{xx}|$. For ^{17}O a value of $e^2Q/h = -6.11$ MHz au^3 was used to convert the q_{zz} output from the Gaussian 98 program into C_Q. It has been noted that computer programs used to calculate EFG tensors can produce a sign difference (−1 factor) depending on how the atomic units eq are treated. The sign of the C_Q values reported in this study were determined by reproducing the experimentally positive C_Q = +10.175 MHz of H_2O (see Table 1).[29,30]

Three general approaches were used to obtain clusters of manageable size for the calculation of the ^{17}O shielding and EFG tensors: (1) We utilized complete clusters based on the primitive cell of the experimentally determined crystal structure, for example, *h*-P_2O_5. This polymorph was a caged structure (P_4O_{10}) and only contained 14 atoms. The cluster is represented by the ball-and-stick portion of Figure 1a. (2) We truncate the crystal structure with O−H in place of O−P bonds. As an example, the *o*-P_2O_5 and *o*′-P_2O_5 structures were composed of interconnecting infinite sheets of phosphate chains, whereas the OH-truncated clusters ($H_6P_4O_{13}$) were chosen to include both the inter- and intrachain bridging oxygen but contained only 23 atoms (Figure 1b,c). For all the OH-truncated clusters based on crystal structures, H atoms were simply inserted in place of specific P atoms prior to the shielding or EFG calculation. No additional geometry optimizations were performed for these OH-truncated clusters. (3) We utilized optimized $H_4P_2O_7$ clusters, where the internal P−O−P angle was varied systematically with no other structural constraints imposed. For all the clusters reported here, C_{2v} symmetry was observed with the TO being eclipsed.

Synthetic and NMR Details. Crystalline $P_2{}^{17}O_5$ was synthesized from powdered elemental red phosphorus (Aldrich) and $^{17}O_2$ gas (Isotec). The gas was enriched to 85% $^{17}O_2$. Ten grams of red phosphorus powder was packed into a glass sublimator inside an argon-filled glovebox and the sublimator was then heated to 300 °C under slight vacuum (0.84 atm). The sublimator was back-filled with $^{17}O_2$ gas to maintain a constant pressure of 1 atm. The $^{17}O_2$ gas reacted with the red phosphorus to produce $P_2{}^{17}O_5$ vapor, which condensed onto the liquid nitrogen coldfinger of the sublimator. Hexagonal $P_2{}^{17}O_5$ was the primary phase that condensed on the coldfinger. This

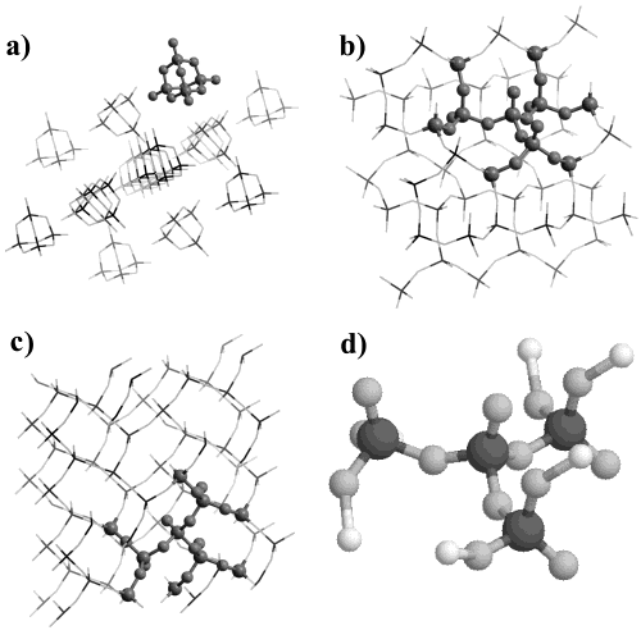

Figure 1. Crystal structures of the three P_2O_5 polymorphs: (a) *h*-P_2O_5; (b) *o*′-P_2O_5; (c) *o*-P_2O_5. The clusters used for the ab initio calculations are shown by the ball-and-stick representation and include the P_4O_{10} cluster in (a), the regions used to generate the OH-terminated $H_6P_4O_{16}$ cluster in (b) and (c), and the $H_6P_4O_{16}$ cluster for *o*′-P_2O_5 in (d). See text for additional details.

material was subsequently twice purified by vacuum sublimation at 300 °C to remove residual elemental phosphorus and other impurities. The purified $P_2{}^{17}O_5$ was stored in sealed glass ampules prior to analysis. Due to the extreme water sensitive nature of P_2O_5, glovebox techniques were used to prevent contamination during packing and storage of the MAS NMR rotor. All of the NMR experiments were preformed using dry N_2 as the spinning gas and the packed rotor was weighed before and after data collection to ensure that no weight gain, due to water uptake, had occurred. Purity was monitored by ^{31}P MAS NMR, which revealed a single resonance at −47.0 ppm.[19] A previous communication from our laboratory incorrectly attributed a second ^{31}P resonance at −35.8 ppm to the inequivalent P site in *h*-P_2O_5, but this has since been determined to be an unidentified impurity.[31] Additionally, no sign of H_3PO_4 was observed in the ^{31}P MAS spectra, which would be expected to be produced due to adsorption of water.

The solid-state ^{17}O MAS NMR spectra were collected at a variety of magnetic field strengths: 9.4, 14.1, and 19.6 T, corresponding to ^{17}O observe frequencies of 54.25, 81.36, and 112.52 MHz, respectively. Typical experimental conditions, as illustrated by the 9.4 T data sets, utilized a Bruker AMX400 spectrometer with a 4 mm broadband probe and a spinning frequency of 15 kHz. The direct ^{17}O acquisition conditions, with no ^1H or ^{31}P decoupling included a 1 μs, 30° pulse, 1024 scan averages, 200 kHz SW (3686 ppm), with a 10 s recycle delay. The ^{17}O MQMAS NMR spectrum was collected at 14.1 T, on a Bruker Avance 600 spectrometer utilizing the three pulse z-filtered MQMAS sequence,[32] spinning at 15 kHz, with optimized pulse lengths of 7.4, 2.0, and 30.0 μs and a 15 s recycle delay. The ^{17}O STMAS NMR spectrum was taken at 112.52 MHz on a Bruker DRX 830 spectrometer, using a three-pulse z-filter sequence,[33,34] with 10 kHz spinning speed, and optimized pulse lengths of 1.0, 1.0, and 3.0 μs. Thirty-two t_1 points were collected with 32 transients for each t_1 point. Extremely careful setting of the magic angle was ultimately set using the *h*-P_2O_5 sample. All of the ^{17}O spectra were externally referenced to neat H_2O (natural abundance) at $\delta = 0.0$ ppm. Simulations of the ^{17}O NMR spectra were performed using the solids analysis program XEDPLOT[35,36] and included second-order quadrupolar contributions to the MAS line shape allowing determinations of the ^{17}O EFG quadrupolar coupling (C_Q) and asymmetry (η_Q) parameter.

Results

P_2O_5 Polymorphs. The crystal structures of the three polymorphs are shown in Figure 1. The hexagonal form (*h*-P_2O_5)[22] is composed of discrete P_4O_{10} adamantoid molecules (Figure 1a). The *o*-P_2O_5 polymorph is composed of interconnected helices of PO_4 tetrahedra forming a three-dimensional network, whereas the *o*′-P_2O_5 polymorph is composed of infinite two-dimensional sheets of corner sharing PO_4 terahedra forming six-membered rings.[23,24] Integral to this study are the bridging oxygen bond angles (P−O−P) found in the various crystalline forms. In *h*-P_2O_5, there are two similar P−O−P bond angles of 122.6° and 123.0°. In *o*-P_2O_5, the two bridging oxygens are very different with P−O−P bond angles of 123.0° and 135.7°. Similarly, the *o*′-P_2O_5 polymorph also contains two dissimilar P−O−P bond angles of 139.9° and 143.7°.

The calculated ^{17}O EFG parameters, C_Q and η_Q, along with isotropic ^{17}O chemical shielding (σ_{iso}) and isotropic chemical shift (δ_{iso}) for the different crystalline polymorphs of P_2O_5 at both HF and B3LYP level of theory are given in Table 1. The ^{17}O δ_{iso} calculations are referenced to H_2O using eq 1, and required no additional scaling. Two different H-terminated $H_6P_4O_{13}$ clusters were simulated for the *o*′-P_2O_5 polymorph, with the clusters centered on the two inequivalent TO (P−O bond lengths of 1.4515 Å and 1.4372 Å, respectively). A normalization factor is generally required for direct comparison of the calculated ^{17}O EFG C_Q, and η_Q values to experimentally determined values. This scaling factor is a function of the level of theory and the basis set utilized in the calculations. It has been argued that the scaling factor for η_Q should be near unity, with the level of theory having only a small impact on the calculated results.[37] As a first approximation, comparison of the ab initio and experimental ^{17}O EFG parameters for H_2O can be used to determine the normalization factor for C_Q. The ab initio EFG calculations for H_2O can utilize either the equilibrium geometry, or a vibration/rotation-corrected equilibrium geometry;[38] results from both H_2O structures are given in Table 1. In the remainder of our discussion, the calculated results obtained from the H_2O equilibrium geometry structure (r_{O-H} = 0.972 Å) were used for the normalization of the predicted ^{17}O C_Q values, because it was found that this geometry correctly predicted the experimental ^{17}O η_Q for H_2O at the B3LYP level of theory (Table 1). The calculated C_Q (normalized by 0.8925 for HF and 0.9242 for the B3LYP calculations) and η_Q for the different oxygen environments in the P_2O_5 polymorphs are given in Table 1, for both HF and B3LYP levels of theory.

The solid-state ^{17}O MAS NMR spectra for crystalline *h*-P_2O_5 taken at different magnetic field strengths, 9.6, 14.1, and 19.6 T, are shown in Figure 2. The reduction in the breadth of the central transition with increasing magnetic field strength is clearly seen in Figure 2 and is indicative of the inverse dependence of the second-order quadrupolar coupling on the magnetic field strength. The ^{17}O MAS NMR second-order quadrupolar broadened central transition spectra were simulated for each magnetic field strength, with the results shown in Figure 3, and the resultant fitting parameters listed in Table 2.

To help distinguish the different oxygen environments, MQMAS and STMAS experiments were also performed. The

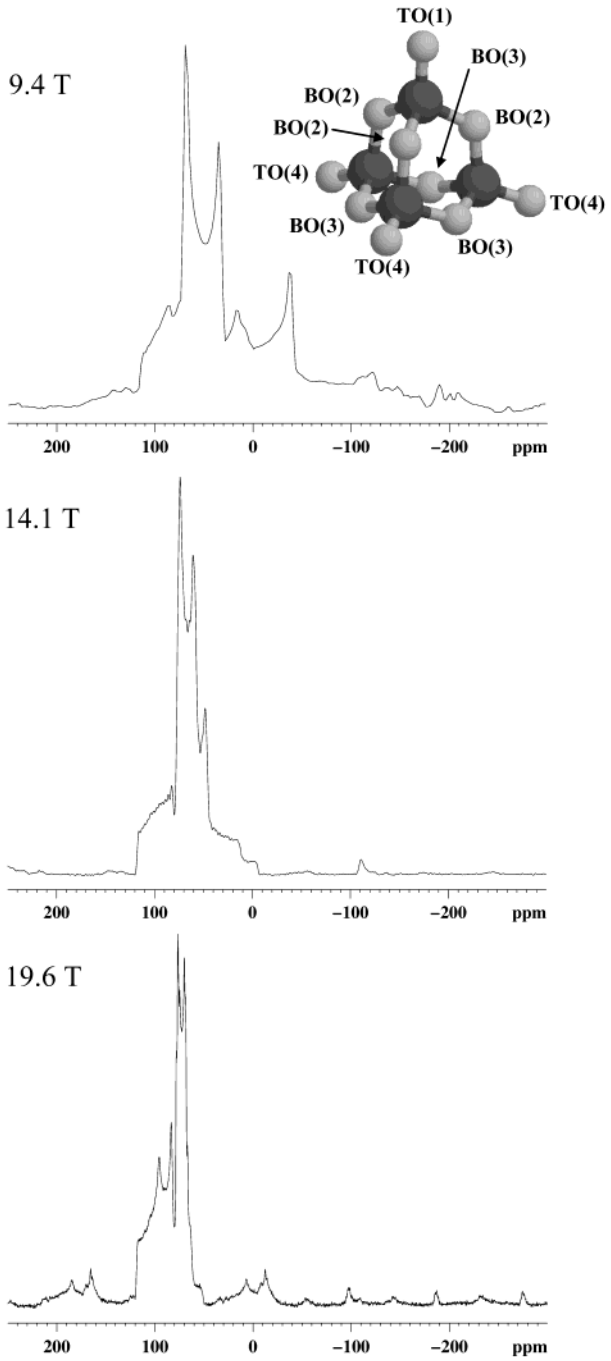

Figure 2. Solid-state ^{17}O MAS NMR spectra for crystalline *h*-P_2O_5 as a function of increasing magnetic field strength. The inset is the adamantoid structure of *h*-P_2O_5, with TO and BO designating the terminal and bridging oxygens, respectively. The numbers correspond to the crystallographic oxygen labels.

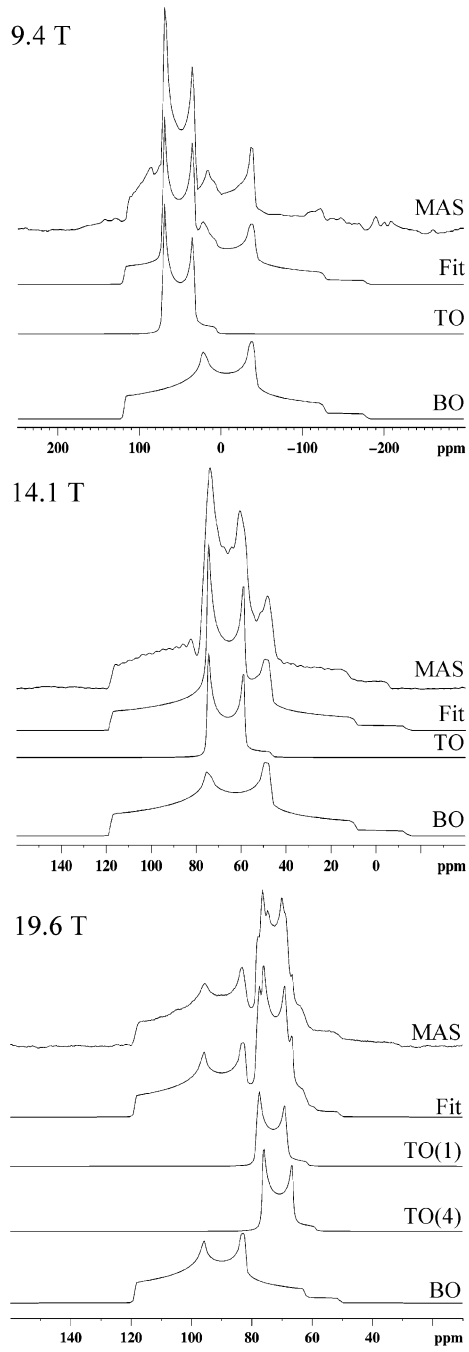

Figure 3. Expanded spectra of the central transition in the ^{17}O MAS NMR of *h*-P_2O_5 as a function of increasing magnetic field strength. Simulated line shapes, including individual contributions from terminal (TO) and bridging (BO) oxygen are shown.

sheared ^{17}O triple quantum (3Q) MQMAS NMR spectrum obtained at 14.1 T is shown in Figure 4. The terminal (TO) oxygen and bridging (BO) oxygen environments are clearly resolved in the MQMAS NMR spectra. Partial resolution of the two TO is also observed in the MQMAS NMR spectra. One-dimensional slices taken through the two peak maximum observed in the isotropic (vertical) dimension, along with the corresponding simulations of the second-order quadrupolar broadened central transition for the TO and BO environments, are shown in Figure 4a,b, respectively. The ^{17}O STMAS NMR spectra of *h*-P_2O_5, taken at 19.6 T, are shown in Figure 5; these data also reveal multiple oxygen environments within the material. The artifact present in the F_2 slice projection of the STMAS data set for the TO (Figure 5b) is due to incomplete suppression of the central transition autocorrelation (CT-CT) diagonal.[33,34]

Correlations between BO C_Q, η_Q, and P−O−P Bond Angle. It is difficult to assess the functional form of the correlation between the ^{17}O EFG and the bridging bond angle based on these limited crystal structure predictions. Therefore, ab initio calculations of the model cluster $H_4P_2O_7$ were investigated in which the EFG parameters of the bridging oxygen were determined for a systematic variation of the P−O−P bond angle. The results for the C_Q (absolute value and normalized) and η_Q from the $H_4P_2O_7$ cluster are shown in Figure 6a,b, respectively. The variation of C_Q as a function of P−O−P bond angle in the $H_4P_2O_7$ cluster was fit to the exponentially

TABLE 2: ^{17}O MAS NMR Quadrupolar Parameters at Multiple Magnetic Field Strengths for *h*-P_2O_5

		C_Q (MHz)	η_Q	δ_{iso} (ppm)	% area CT
9.4 T	TO	3.86 ± 0.2	0.0 ± 0.05	81.1 ± 1	34
	BO	7.47 ± 0.2	0.6 ± 0.05	125.6 ± 2	66
14.1 T	TO	3.82 ± 0.2	0.0 ± 0.05	79.5 ± 1	30
	BO	7.48 ± 0.2	0.6 ± 0.05	121.0 ± 2	70
19.6 T	TO(1)	4.13 ± 0.2	0.0 ± 0.05	79.1 ± 1	15
	TO(4)	4.03 ± 0.2	0.1 ± 0.05	80.8 ± 1	24
	BO	7.42 ± 0.2	0.6 ± 0.05	120.3 ± 2	61
av	TO	3.96 ± 0.2	0.00 ± 0.05	80 ± 1	
	BO	7.46 ± 0.2	0.60 ± 0.05	122 ± 2	

parameterized empirical relationship defined by

$$|C_Q(\theta)| = a\left(\frac{1}{2} + \frac{\cos\theta}{\cos\theta - 1}\right)^{\alpha} \qquad \theta' \le \theta \le 180 \quad (4a)$$

$$|C_Q(\theta)| = a(\cos\theta) + b \qquad 100 \le \theta < \theta' \quad (4b)$$

where the angle $\theta' \sim 116.75°$ for the HF calculations and $\theta' \sim 117.25°$ for the B3LYP calculations. The HF results are described by $a = 10.14$ and $\alpha = 1.64$ for $116.75° \le \theta \le 180°$ (eq 4a) and $a = 6.62$ and $\alpha = 10.09$ for $100° \le \theta < 116.75°$ (eq 4b), whereas the B3LYP results are fit by $a = 10.11$ and $\alpha = 1.80$ for $117.25° \le \theta \le 180°$ (eq 4a) and $a = 5.52$ and $\alpha = 9.45$ for $100° \le \theta < 117.25°$ (eq 4b). There is a sign change in C_Q at θ' (positive for $\theta < \theta'$, and negative $\theta > \theta'$) due to the change in the EFG orientation at this angle. For the remainder of the discussion we will be concerned with the absolute value of C_Q. The parametrized exponent expression given in eq 4a was originally proposed by Vermillion et al.[13] and has subsequently been used to describe C_Q variations for a variety of inorganic oxide clusters.[14,37]

The variation of η_Q with the P−O−P bond angle in the $H_4P_2O_7$ cluster was fit to an exponential-parametrized expression given by

$$\eta_Q(\theta) = a\left(\frac{1}{2} - \frac{\cos\theta}{\cos\theta - 1}\right)^{\alpha} + b \qquad \theta' \le \theta \le 180° \quad (5a)$$

$$\eta_Q(\theta) = a\cos\theta + b \qquad 100° \le \theta < \theta' \quad (5b)$$

where again the angle $\theta' \sim 116.75°$ for the HF calculations and $\theta' \sim 117.25°$ for the B3LYP calculations. The variation of the HF η_Q calculations were fit by $a = 6.95$, $b = 0.04$, and $\alpha = 1.21$ for $116.75° \le \theta \le 180°$ (eq 5a) and $a = -3.52$ and $b = -0.58$ for $100° \le \theta < 116.75°$ (eq 5b), whereas the B3LYP results were fit by $a = 6.64$, $b = 0.06$, and $\alpha = 1.18$ for $117.25° \le \theta \le 180°$ (eq 5a) and $a = -3.49$ and $b = -0.59$ for $100° \le \theta < 117.25°$ (eq 5b). These empirical fits are shown in Figure 6b by the solid and dashed lines for HF and B3LYP, respectively. Note that for $100° \le \theta < 117.25°$ the fits to the HF and B3LYP results are indistinguishable (Figure 6b). Variations in C_Q and η_Q as a function of P−O−P bond angle in the P_2O_5 polymorphs are also shown in Figure 6a,b as filled and unfilled symbols for HF and B3LYP methods, respectively. The analytical expression given in eq 5a ($\theta > \theta'$) is equivalent to eq 25 in Vermillion et al.[13] presented for silicates where they defined a term $\Delta\eta_q^M$ to described the offset due to some alkali metal cation at an equilibrium orientation. Though mathematically equivalent, the expressions in eqs 5a and 5b do not include offsets from cation contributions but describe the predicted η_Q variations within the $H_4P_2O_7$ clusters (without any coordinating cations). The additional impact of cations and their orientations of the resultant correlation of C_Q and η_Q versus the bridging P−O−P bond angle will be further detailed in a later paper.[39]

The variation of the predicted C_Q (normalized) versus η_Q for the $H_4P_2O_7$ cluster is shown in Figure 7a. The functional form of this variation is different for P−O−P angles greater than or less than the critical θ', as noted in eqs 4 and 5. For the HF level of theory (solid symbols Figure 7a) the predicted correlation between C_Q and η_Q is analytically described by the second-order polynomial ($C_Q = b_0 + b_1\eta_Q + b_2\eta_Q^2$) with $b_0 = +9.04$, $b_1 = -2.25$, and $b_2 = +0.379$ for $\theta < \theta'$ and $b_0 = +10.29$, $b_1 = -4.33$, and $b_2 = +1.21$ for $\theta > \theta'$. For the B3LYP level of theory the predicted variation between C_Q and η_Q is also described by a second-order polynomial with $b_0 = +8.52$, $b_1 = -1.64$, and $b_2 = +0.06$ for $\theta < \theta'$ and $b_0 = +10.37$, $b_1 = -4.73$, and $b_2 = +1.31$ for $\theta > \theta'$.

In many instances the quadrupolar coupling product (P_Q) is obtained from the experimental NMR measurements (especially true in amorphous systems) instead of the individual EFG parameters C_Q and η_Q. The coupling product is defined by

$$P_Q = C_Q\sqrt{1 + \frac{\eta_Q}{3}} \quad (6)$$

The variation of the predicted P_Q (absolute value) with P−O−P bond angle for the bridging oxygen in the $H_4P_2O_7$ cluster is shown in Figure 7b. The variation in the predicted C_Q and η_Q values and the resulting P_Q fit utilized the empirical relationships given in eqs 4a, 4b, 5a, 5b, and 6.

Discussion

P_2O_5 Polymorphs. The ab initio calculations for the different polymorphs of P_2O_5 demonstrate that the ^{17}O NMR parameters can be used to identify the various oxygen environments in these systems. For example, in the experimental ^{17}O MAS NMR of *h*-P_2O_5 reported here (Figures 2 and 3, Table 2) at least two types of oxygen resonances are observed, one with a large C_Q of ∼7.5 MHz, $\eta_Q \sim 0.6$ and a isotropic chemical shift of ∼ +122 ppm, and a second oxygen resonance with a much smaller C_Q of ∼4.0 MHz, $\eta_Q \sim 0$ and an isotropic chemical shift of ∼ +80 ppm (Table 2). In Table 1 the predicted C_Q (normalized) values for the terminal oxygens (TO) in the different polymorphs of P_2O_5 range from approximately −4.1 to −4.5 MHz, whereas the predicted C_Q's of the bridging oxygens (BO) range from approximately −7.6 through −9.1 MHz. For the P_2O_5 polymorphs investigated, the sign of calculated C_Q was determined to be negative, consistent with previous results in silicate, alumiosilicate, aluminate, and germanate clusters. Experimentally, the ^{17}O MAS NMR results only allow the absolute magnitude of C_Q to be determined, such that the negative sign determined in the ab initio calculations is dropped for comparisons. The results of these calculations allow the separation and assignment of the TO and BO oxygen signals observed in *h*-P_2O_5, simply based on the magnitude of C_Q. Similar arguments were made by Zeyer et al.[20] for the assignment of the BO and the nonbridging P—O—Na oxygen (NBO) ^{17}O NMR signals in $Na_2O-P_2O_5$ glasses. Zeyer used the relationship between C_Q and the average bond ionic character (I %) proposed by Schramm and Oldfield,[40] to predict C_Q for the BO (P—O—P) of ∼7.4 MHz, and ∼3.7 MHz for the NBO (P—O—Na^+). The predicted C_Q for the BO is very close to the 7.46 MHz value observed experimentally in *h*-P_2O_5 (Table 2), but a little smaller than the C_Q predicted for the other P_2O_5 polymorphs in Table 1. The experimentally measured C_Q (∼4.0 MHz) for the TO in *h*-P_2O_5 (Table 2) is significantly lower that

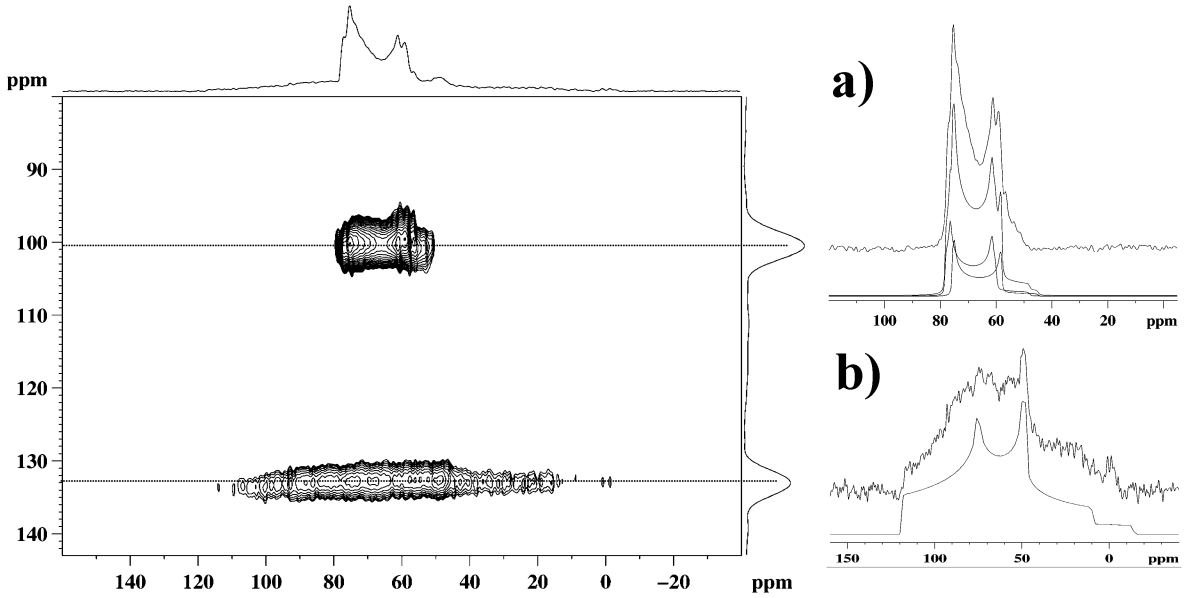

Figure 4. Solid-state ^{17}O MQMAS NMR of *h*-P_2O_5 at 14.1 T. The upper projection is the MAS dimension, and the projection to the right is the isotropic dimension. The 1D slices taken at the isotropic peak maxima reveal the individual second-order quadrupolar-broaden spectra for the (a) terminal (TO) and (b) bridging (BO) oxygen sites. Fit to the 1D slices are based on the fit to the MAS NMR spectra.

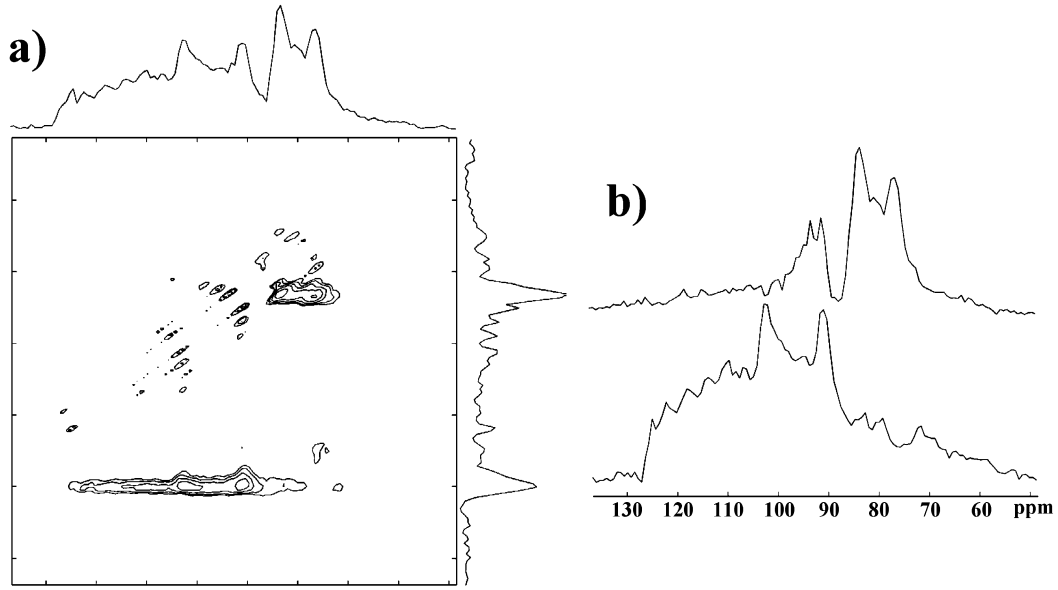

Figure 5. (a) Solid-state ^{17}O 2D STMAS NMR spectrum of *h*-P_2O_5 after shearing and skyline projections along both dimensions. (b) F_2 slice projections of the terminal (TO) and bridging (BO) ^{17}O sites of *h*-P_2O_5.

the C_Q (∼4.8 MHz) observed for the NBO in the $Na_2O-P_2O_5$ glasses, even though the predicted C_Q (∼3.7 MHz) based on electronegativities for the NBO[20] is very similar to the value observed experimentally for the TO. It should be noted that the ionic character−C_Q relationship forwarded by Schramm and Oldfield is not directly applicable to predicting TO values. For the sodium phosphate glass compositions investigated by Zeyer et al.[20] signals from terminal oxygen (TO) environments (P═O) were not observed but are not predicted to be present in significant concentrations. To date no relationship between the ^{17}O NMR C_Q and the P—O—P bond angle has been reported, but it can be seen in Table 1 that the bond angle clearly influences the magnitude of C_Q. A detailed discussion of developing correlations between bond angle and C_Q is presented below.

The empirical relationship for C_Q given in eq 4a ($\theta > \theta'$) is identical to that put forward by Vermillion et al. to describe C_Q variations in silicate clusters. The fitted *a* parameters for the phosphate clusters are ∼3 MHz larger (in absolute value) than that observed in silicates, whereas the α values (which range between 1.64 and 1.80 for HF and B3LYP) are similar to α = 1.71 reported in silicates.[13] The larger C_Q values for ^{17}O in phosphates in comparison to silicates was noted in the early investigations of $P_3O_9^{3-}$ anion and was attributed to the more ionic character of the Si−O bond. This observation is also consistent with the empirical correlation between C_Q and ionic character proposed by Schramm and Oldfield.[40] No equivalent empirical relationship for C_Q has been reported for $\theta < \theta'$ (eq 4a) in silicate clusters. For phosphates, bridging P−O−P bond angles smaller than ∼120° do not appear to readily occur in natural materials. However, recent ab initio calculations[41] on strained phosphate ring clusters have predicted P−O−P bond angles of ∼95° for the highly strained phosphate rings contain-

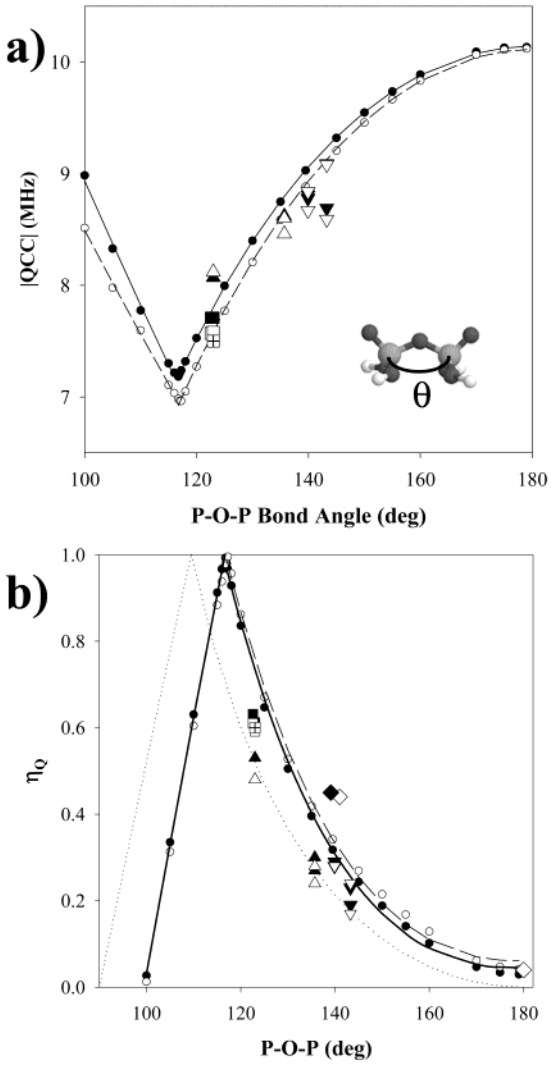

Figure 6. Variations in the ^{17}O EFG (a) C_Q and (b) η_Q as a function of the P−O−P bond angle for the bridging oxygen in the $H_4P_2O_7$ cluster are shown. The calculated values (● = HF, ○ = B3LYP) and the corresponding empirical fits (using eqs 4 and 5) are given by solid and dashed lines for the HF and B3LYP level of theory, respectively. The dotted line in (b) corresponds to the relationship given by eq 7. The predicted values of C_Q and η_Q for the different P_2O_5 polymorphs are also given: (■, □) *h*-P_2O_5, (▲, △) *o*-P_2O_5, and (▼, ▽) *o*′-P_2O_5, with the filled and unfilled symbols corresponding to HF and B3LYP level of theory. The symbol (◇) shows the η_Q values previously reported for select $H_4P_2O_7$ clusters by Clark and Gradinetti,[14] whereas (◆) is for the $P_3O_9^{3-}$ cluster reported by Lindsay and Tossell.[12] The experimentally values determined by ^{17}O NMR for *h*-P_2O_5 are given by (⊞).

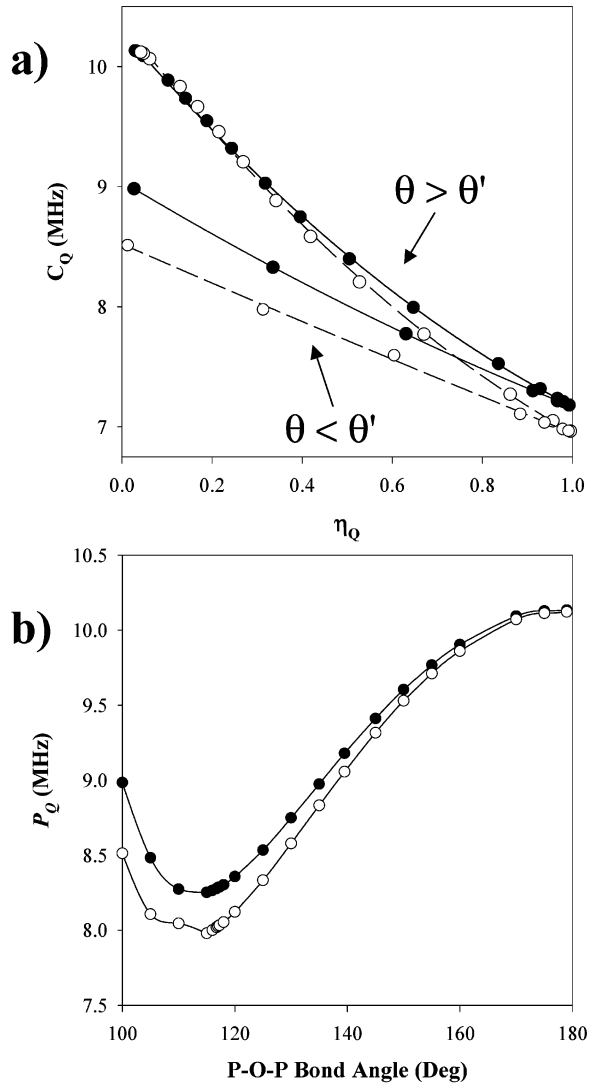

Figure 7. (a) Correlation between the ^{17}O EFG C_Q and η_Q at both (●) HF and (○) B3LYP levels of theory. (b) Variations in the ^{17}O quadrupolar product P_Q with the bridging oxygen P−O−P bond angle at (●) HF and (○) B3LYP levels of theory.

ing two phosphate groups. For rings composed of three phosphate groups the P−O−P bond angles were predicted to range from 121° to 139°. These empirical relationships for the smaller P−O−P bond angles may provide a means for using ^{17}O MAS NMR to identify the existence of highly strained phosphate ring clusters in amorphous ultraphosphate materials.

Similar differentiation of the TO and BO ^{17}O NMR signals in *h*-P_2O_5 can also be made on the basis of the asymmetry of the EFG tensor. It is predicted (Table 1) that the TO ^{17}O EFG tensors are nearly symmetric ($\eta_Q \sim 0$) in *h*-P_2O_5 and *o*-P_2O_5. The η_Q values in *o*′-P_2O_5 show a little larger asymmetry ($\eta_Q < 0.16$). Simulations of *o*-P_2O_5 and *o*′-P_2O_5 using a smaller H-terminated $H_5P_3O_{10}$ cluster (versus the $H_6P_4O_{13}$ cluster presented in this paper) predicts a much larger asymmetry ($\eta_Q \sim 0.5$), demonstrating that cluster size directly influences the EFG asymmetry calculations. The $H_4P_2O_7$ cluster investigated below shows a similar magnitude of the predicted η_Q for the TO. For this reason only the results for the TO in the center of the H-terminated $H_6P_4O_{13}$ cluster are reported in Table 1. Future experimental determination of η_Q for *o*-P_2O_5 and *o*′-P_2O_5 will allow a basis on which to address issues of cluster size and H-truncation errors in the ab initio calculations for these systems. Correlations between the TO η_Q and adjacent bond angles, asymmetry in bonding, and P−O bond distances based on ab initio calculations will be explored elsewhere.[39] In addition, the bridging oxygen η_Q's in *h*-P_2O_5 are much larger ($\eta_Q > 0.6$), whereas in *o*-P_2O_5 and *o*′-P_2O_5 η_Q values are smaller and more varied, ranging from 0.16 to 0.53. The variation of η_Q with the bridging P−O−P bond angle is also evident (Table 1). The development of correlations between bridging bond angle and η_Q for the BO is discussed below.

The ab initio calculation of the isotropic chemical shift (δ_{iso}) for the different P_2O_5 polymorphs predict a range of differences between TO and BO environments (Table 1). In *h*-P_2O_5 it is predicted that there is approximately +20 ppm difference in δ_{iso} between the TO and BO, with the BO having the larger δ_{iso} value. Experimentally, the δ_{iso} difference between TO and BO in *h*-P_2O_5 is significantly larger at ∼+42 ppm. The

predicted δ_{iso} values for the *o*-P_2O_5 and *o*′-P_2O_5 polymorphs (Table 1) show an inconsistent distinction between TO and BO. The differences between the predicted δ_{iso} TO and BO varies with the level of theory used in the calculations and with the specific cluster investigated (see Table 1). Presently there is no experimental measure of δ_{iso} for the *o*-P_2O_5 and *o*′-P_2O_5 polymorphs. The discrepancy between ab initio predicted ^{17}O δ_{iso} values and experiment has been noted before and is most likely the result of truncation of the surrounding atom shells during the selection of the limited-size cluster used for the NMR calculations. For example the δ_{iso} of the central TO in the $H_6P_4O_{13}$ clusters is $\sim +30$ ppm larger than the calculated δ_{iso} of the TO groups that are adjacent to terminating OH species within the same cluster. In previous calculations of ^{17}O δ_{iso} values in SiO_2 polymorphs, Xue and Kanzaki[42] demonstrated that larger cluster models that include second neighbor atoms with respect to the oxygen of interest are required for correct convergence of the ^{17}O NMR δ_{iso} calculations. The *o*- and *o*′-P_2O_5 polymorphs are periodic network structures, and thus truncation to form clusters will produce errors in the calculated chemical shifts. For the *h*-P_2O_5 polymorph these same cluster truncation effects are not as important (due to the adamantoid type primitive cell); however, the calculation of δ_{iso} for the TO in *h*-P_2O_5 may be further improved (or reach convergence) by including additional copies of the primitive cell to form even larger clusters. The development and calculation of these larger clusters was not pursued in the present study. It is felt that the large difference in predicted δ_{iso} between the TO and BO should allow for the correct assignment of these two types of oxygen environments but cannot be used to distinguish the inequivalent TO or the inequivalent BO present in *h*-P_2O_5 (see discussion below). Presently it is not clear if a general argument can be made to distinguish between TO and BO in other phosphate systems. Further experimental data for different phosphates along with modeling of larger clusters will be needed to clarify such generalizations.

The assignment of the TO and BO in *h*-P_2O_5 to the ^{17}O MAS NMR resonances can be done consistently using all three ^{17}O parameters, C_Q, η_Q, and δ_{iso}, and is detailed in Table 2. The average of these different fits for the three magnetic field strengths shows that the TO is characterized by $C_Q = 3.96 \pm 0.2$ MHz, $\eta_Q = 0.00 \pm 0.1$, and $\delta_{iso} = 80 \pm 1$ ppm, whereas the BO is characterized by $C_Q = 7.46 \pm 0.2$ MHz, $\eta_Q = 0.60 \pm 0.1$, and $\delta_{iso} = 122 \pm 2$ ppm. The TO and the BO environments are also clearly distinguished in the MQMAS and the STMAS spectra shown in Figures 4 and 5. The 1D slices taken through the MQMAS data (Figures 4a and 5b) allow the line shapes of the TO and BO to be observed without the overlap that occurs in the 1D MAS spectra (Figures 2 and 3). The difficulty in exciting and reconverting the 3Q coherence for oxygen sites with large C_Q values and lower radio frequency power has been discussed previously[43−45] and gives rise to the poor signal-to-noise observed in the MQMAS slice through the BO ($C_Q \sim 7.5$ MHz) seen in Figure 4b. There was some concern about the observation of multiple BO sites in the MQMAS due to poor excitation, so a STMAS experiment at 19.6 T was also performed. Cross-peaks in STMAS are not strongly dependent on the C_Q values, such that excitation of the BO is readily apparent. The P_Q values obtained for the TO and BO from the MQMAS and STMAS experiments are consistent with the average C_Q and η_Q results given in Table 2.

On the basis of the crystal structure of *h*-P_2O_5, there are four inequivalent oxygen environments (see Figures 1 and 2), two TO environments (in a ratio of 3:1), and two BO environments (in a 3:3 ratio). The question remains if these inequivalent TO and BO sites can be resolved in the experimental ^{17}O NMR spectra. Based on the 1D MAS ^{17}O NMR spectra (Figures 2 and 3), observation of these multiple inequivalent sites is not readily apparent. Close inspection of the ^{17}O MAS spectra at 19.6 T (Figure 3c) indicates that the region assigned to the TO is in fact the superposition of two second-order quadrupole patterns. These TO resonances differ by 0.1 MHz in C_Q, 0.1 in η_Q, and 0.9 ppm in δ_{iso}. We assign these as TO(1) and TO(4) on the basis of the ab initio C_Q calculations for *h*-P_2O_5 (Table 1). Distinctions based on η_Q or δ_{iso} are not warranted because the experimental differences are on the order of experimental error. TO(1) corresponds to the crystallographic oxygen site (O1) that caps the cage structure, and TO(4) is tentatively assigned to the crystallographic oxygen site (O4), which are the three TO of the PO_4 tetrahedra forming the base of the P_4O_{10} cage.[22] Assignment based solely on the relative intensities is difficult for samples containing multiple sites with vastly different C_Q. For quadrupolar nuclei, the intensity of the center NMR resonance may contain contributions from transitions other than the $+1/2 \rightarrow -1/2$ transition and is dependent on the ratio of the quadrupolar frequency ($\upsilon_Q = 3C_Q/2I[2I - 1]$), the applied radio frequency (υ_{rf}), and the excitation bandwidth.[36,46] The relative intensities listed in Table 2 are based solely on integration of the central resonance and were not corrected, for intensity contributions from these effects. At higher field strengths, these effects will become less pronounced such that the relative population of the TO and BO at 19.6 T (Table 2) is very close to that found in the crystal structure.

It is interesting to note that the two different TO environments are only partially resolved in the MQMAS spectra obtained at 14.1 T (Figure 4a). Unfortunately, MQMAS data at 19.6 T were not available. In addition, the two inequivalent BO are not resolved in either the MQMAS or the STMAS experiments. From the ab initio calculations presented in Table 1, it is predicted that C_Q and η_Q for *h*-P_2O_5 are almost identical for these different BO environments, suggesting that they may be experimentally difficult to resolve even at the high fields employed in the present study.

Tables 1 and 2 (and Figure 6) reveal that even by normalizing to H_2O at the same level of theory there are differences in the predicted C_Q up to 0.2 MHz obtained using either HF or B3LYP methods. It is also interesting to note that there are small differences in the predicted η_Q values when HF versus B3LYP calculations are compared, resulting from small differences in the distribution of charge within the oxygen systems. Recall that these calculations were based on primitive cell structures or H-terminated clusters obtained from the corresponding crystal structures, such that there were no geometry optimizations performed. The observation of differences in η_Q between theory level (HF versus B3LYP) is in contrast to the argument of Clark and Grandinetti[37] that η_Q would be relatively insensitive to the calculation method because η_Q is a ratio of the principal components of the EFG tensor (eq 3). Because the experimental results of the present study provide only one crystalline compound to refine and/or adjust the predicted C_Q and η_Q values, no additional corrections to the normalization factor beyond that of scaling C_Q to experimental values of H_2O are warranted at this time, even though the B3LYP method predicted values that were more consistent with the experimental results. Additional experimental measurements of the ^{17}O NMR parameters for different crystalline phosphate compounds will allow modification of the normalization factor.

Correlations between Bridging Oxygen C_Q, η_Q, and the P−O−P Bond Angle. Theoretical and experimental investigations of correlation involving the ^{17}O NMR EFG parameters in phosphates are very limited. To date no relationship has been developed for the variation of C_Q as a function of bridging oxygen bond angle in phosphates, even though Lindsay and Tossell demonstrated that the magnitude of the EFG increased with increasing P−O−P bond angle in the $H_3POPH_3^{2+}$ cluster over a decade ago.[12] Equations 5a and 5b along with Figure 6a show the resulting C_Q versus P−O−P bond angle correlations developed in this paper. There is a general increase in the absolute magnitude of C_Q with increasing P−O−P above θ' (∼117°), or an almost linear increase in C_Q with decreasing P−O−P bond angle below θ'. The experimental values obtained for *h*-P_2O_5 agree very well with the C_Q correlation obtained using the B3LYP level of theory (results are within experimental error of ±0.2 MHz). The predicted variation of C_Q with P−O−P bond angle for the P_2O_5 polymorphs (Figure 6a) is also in general agreement with the trend of the developed C_Q correlation.

The variation of η_Q with bond angle in bridging oxygens (BO) has been more extensively investigated. Sternberg[47] derived an empirical relationship between η and the X−O−X (X = Si, P) bond angle assuming only σ-bonding in the symmetric X−O−X linkage, given by

$$\eta(\theta) = -\frac{3(3\cos\theta + 1)}{3\cos\theta - 1} \qquad 109.47° \le \theta \le 180°$$

$$\eta(\theta) = -3\cos\theta \qquad 90° \le \theta < 109.47° \qquad (7)$$

The dotted line in Figure 6b shows the variation of η_Q with the P−O−P bond angle given by this relationship. Grandenetti[48] later demonstrated that this η_Q relationship remains valid even for cases involving d−p π bonding, if the occupancy of the third and fourth occupied orbital remains equal. The relationship is expected not to apply to situations where the C_{2v} of D_2 symmetry is removed (asymmetric linkages), or to systems where there is extensive d−p π bonding. These predicted correlations between η_Q and the P−O−P bond angle have not been experimentally verified in phosphate systems. The experimental value of $\eta_Q = 0.60$ for *h*-P_2O_5 (Table 2) is slightly larger than the η_Q predicted using eq 7 but is smaller than the η_Q correlation given by eq 5a. For *h*-P_2O_5 (P−O−P ∼ 123°) the experimental $\eta_Q = 0.6$ would correspond to a P−O−P bond angle of 120° using eq 7 and 128° using eq 5a (at B3LYP level of theory). The η_Q values predicted for the *o*-P_2O_5 polymorph are well represented by eq 7, whereas, interestingly, the η_Q values for the *o*′−P_2O_5 polymorph are better predicted by the correlation in eq 5a. The η_Q values predicted for the $H_4P_2O_7$ cluster by Clark and Grandinetti[14] or the $P_3O_9^{3-}$ cluster by Lindsay and Tossell[12] are in better agreement with the η_Q correlation presented in the present study (eq 5a).

In the $H_4P_2O_7$ cluster η_Q was calculated to have a nonzero value as θ approaches 180°. This is a result of the asymmetric environment produced by the terminal oxygen present on the linking phosphorus group. A similar offset was also calculated by Clark and Grandinetti for the $\theta = 180°$ configuration of the $H_4P_2O_7$ cluster (diamond symbol in Figure 6a). These long-range structural effects in the $H_4P_2O_7$ clusters result from the presence of terminal P═O bonds with significant oxygen π-bonding within the cluster. This difficulty does not appear to occur in the analogous silicate, germanate, and aluminate clusters. These long-range structural effects on the ^{17}O EFG tensor in phosphates will be discussed in more detail elsewhere, including the effect of neighboring OH species (Alam in preparation). In the limit $b = 0$ the $\theta' \le \theta \le 180°$ relationship in eq 5a is equivalent to eq 13 Vermillion et al.[13] proposed for silicate clusters, but in the case of phosphate clusters, an offset is required to accurately fit the nonzero η_Q observed for $\theta = 180°$ configurations. Not surprisingly, the values of *a* and α parameters obtained from the fitting of the η_Q variation in the phosphate cluster (eq 5a) are very similar to the values reported for the fitting of the η_Q variation in analogous silicate clusters.

The variation of C_Q versus η_Q (Figure 7a) was found to be nonlinear in both P−O−P bond angle regimes investigated. This nonlinear behavior is in contrast to the linear variation predicted for analogous silicate cluster Si−O−Si bond angles greater 120°. In the $H_4P_2O_7$ cluster the nonlinear dependence is most likely due to the influence of the two TO species within the cluster and the impact of π-bonding on the BO EFG parameters. This nonlinear variation between C_Q and η_Q precludes the development of simple expressions for the modeling of C_Q and η_Q distributions in disordered systems. The correlation in Figure 7 can also be used to exclude possible combinations of C_Q and η_Q during the analysis and simulation of the ^{17}O NMR spectra where multiple combinations are possible (especially in disordered systems or static spectra). For example, for values of $\eta_Q < 0.5$, the magnitude of C_Q must be greater than ∼7.8 MHz (for small P−O−P bond angles) and greater than ∼8.4 MHz for the larger P−O−P bond angles.

Although the $H_4P_2O_7$ cluster was developed to represent phosphate systems containing terminal oxygen (TO) environments, it is interesting (though not rigorously valid) to discuss the recent ^{17}O NMR result for the BO of sodium phosphate glasses, xNa$_2$O·$(1-x)$P$_2$O$_5$ (x = 0.465−0.628) presented by Zeyer and co-workers.[20] With increasing sodium concentration, they found that both P_Q and C_Q of the BO decreased, whereas η_Q of the BO increased. From Figures 6 and 7 these changes suggest a decrease in the average P−O−P bond angle with increasing sodium concentration. From the P_Q correlation in Figure 7, the 8.4−8.1 MHz reported for the 46.5−56.3% Na_2O glass (obtained from the MQMAS spectra) corresponds to P−O−P angles ranging from 120° to 128°. The $P_Q = 7.0$ MHz for the 62.8% Na_2O glass is below the minimum value predicted in Figure 7b, suggesting problems with attempting to project the results of the $H_4P_2O_7$ cluster to this compositional range, which contains only ∼16% BO and no TO environments. The C_Q values reported for the 46.5−56.3% Na_2O glass range from 7.8 to 7.6 MHz, corresponding to P−O−P angles ranging from 121° to 126° on the basis of the B3LYP correlation shown in Figure 6a. The η_Q values for this same glass compositional range (η_Q = 0.35−0.38) would predict a much larger P−O−P bond angle on the basis of the correlations in Figure 6b and eq 6, ranging from 136° to 138°. A P−O−P bond angle of a bond angle of 126° for the 62.8% sodium phosphate glass, and ∼130° for the rest of the compositions studied is predicted using the Sternberg relationship in eq 7. A P−O−P bond angle of 137 ± 3° has been determined from XRD measurements in υ-P_2O_5,[49] but extraction of the P−O−P bond angle in modified glasses using the same method has not been reported.[50] The difference in the predicted P−O−P angles obtained using either C_Q or η_Q correlations may result from variations in these parameters with the introduction of cations into the system. In silicate systems it has been shown that the magnitude of C_Q decreases with each cation introduced into the neighboring sphere of the BO, whereas η_Q increases with the first cation introduced, but then partly decreases in magnitude with the second cation introduction.[13]

Similar variations are expected for phosphate systems and will be the focus of future research.

Conclusion

In summary, through the combined use of ^{17}O MAS NMR at multiple magnetic field strengths along with the 2D MQMAS and STMAS NMR experiments, a relatively complete description of the ^{17}O NMR parameters for *h*-P_2O_5 has been obtained. These results for a material with a well-defined crystal structure provide experimental verification of the ab initio theoretical predictions for the three different polymorphs of P_2O_5. From the analysis of the predicted ^{17}O EFG parameters in the $H_4P_2O_7$ cluster empirical correlations between the bridging oxygen (P−O−P) bond angle and EFG parameters C_Q, η_Q, and P_Q were determined. The empirical relationships obtained between the EFG parameters C_Q and P_Q, and the bridging P−O−P bond angle are the first reported for phosphate systems. The η_Q correlations obtained are slightly different from the empirical correlations previously used for analysis of ^{17}O NMR asymmetry parameters in phosphate systems.

Acknowledgment. We thank Steve Martin for initial synthetic work on ^{17}O labeling of *h*-P_2O_5, along with Phil Gradinetti and Christian Jäger for helpful discussions. This work is partially supported by the DOE Office of Basic Energy Sciences (OBES). Sandia is a multiprogram laboratory operated by Sandia Corporation, a Lockheed Martin Company, for the United States Department of Energy under contract DE-AC04-94AL85000.

References and Notes

(1) Clark, T. M.; Grandinetti, P. J.; Florian, P.; Stebbins, J. F. *J. Phys. Chem. B* **2001**, *105*, 12257.
(2) Farnan, I.; Grandinetti, P. J.; Baltisberger, J. H.; Stebbins, J. F.; Werner, U.; Eastman, M. A.; Pines, A. *Nature* **1992**, *358*, 31.
(3) Cong, X. D.; Kirkpatrick, R. J. *J. Am. Ceram. Soc.* **1996**, *79*, 1585.
(4) Maekawa, H.; Florian, P.; Massiot, D.; Kiyono, H.; Nakamura, M. *J. Phys. Chem.* **1996**, *100*, 5525.
(5) Mueller, K. T.; Baltisberger, J. H.; Wooten, E. W.; Pines, A. *J. Phys. Chem.* **1992**, *96*, 7001.
(6) Stebbins, J. F.; Oglesby, J. V.; Xu, Z. *Am. Miner.* **1997**, *82*, 1116.
(7) Xue, X. Y.; Stebbins, J. F.; Kanzaki, M. *Am. Miner.* **1994**, *79*, 31.
(8) Zhao, P. D.; Kroeker, S.; Stebbins, J. F. *J. Non-Cryst. Solids* **2000**, *276*, 122.
(9) Kubicki, J. D.; Topkis, M. J. *Am. Miner.* **2002**, *87*, 668.
(10) Tossell, J. A.; Lazzeretti, P. *Chem. Phys. Lett.* **1987**, *112*, 205.
(11) Tossell, J. A.; Lazzeretti, P. *Phys. Chem. Miner.* **1988**, *15*, 564.
(12) Lindsay, C. G.; Tossell, J. A. *Phys. Chem. Miner.* **1991**, *18*, 191.
(13) Vermillion, K. E.; Florian, P.; Grandinetti, P. J. *J. Chem. Phys.* **1998**, *108*, 7274.
(14) Clark, T. M.; Grandinetti, P. J. *Solid State Nucl. Magn. Reson.* **2000**, *16*, 55.
(15) Wu, G.; Rovnyak, D.; Huang, P. C.; Griffin, R. G. *Chem. Phys. Lett.* **1997**, *277*, 79.
(16) Kyung, H.; Timken, C.; Turner, G. L.; Lambert, S. L.; Welsh, L. B.; Oldfield, E. *J. Am. Chem. Soc.* **1986**, *108*, 7236.
(17) Kozhevnikov, I. V.; Sinnema, A.; Van Bekken, H.; Fournier, M. *Catal. Lect.* **1996**, *41*, 153.
(18) Witschas, M.; Eckert, H.; Freifeit, H.; Putnis, A.; Korus, G.; Jansen, M. *J. Phys. Chem. A* **2001**, *105*, 6808.
(19) Grimmer, A. R.; Wolf, G. U. *Eur. J. Solid State Inorg. Chem.* **1991**, *28*, 221.
(20) Zeyer, M.; Montagne, L.; Kostoj, V.; Palavit, G.; Prochnow, D.; Jaeger, C. *J. Non-Cryst. Solids* **2002**, *311*, 223.
(21) Montagne, L.; Palavit, G.; Lefert, R.; Amoureux, J. P.; Zeyer, M.; Jaeger, C. *^{17}O Multi-Quantum NMR of Phosphate Glasses*; International Congress on Glass: Edinburgh, Scotland, 2001.
(22) Jansen, M.; Luer, B. *Z. Kristal.* **1986**, *117*, 149.
(23) Arbib, E.-H.; Elouadi, B.; Chaminade, J.-P.; Darriet, J. *J. Solid State Chem.* **1996**, *127*, 350.
(24) Stachel, D.; Svoboda, I.; Fuess, H. *Acta Crystallogr.* **1995**, *C51*, 1049.
(25) Frisch, M. J.; Trucks, G. W.; Schlegel, H. B.; Scuseria, G. E.; Robb, M. A.; Cheeseman, J. R.; Zakrezewski, V. G.; Montgomery, J. A.; Stratmann, R. E.; Burant, J. C.; Dapprich, S.; Millam, J. M.; Daniels, A. D.; Kudin, K. N.; Strain, M. C.; Farkas, O.; Tomasi, J.; Barone, V.; Cossi, M.; Cammi, R.; Mennucci, B.; Pomelli, C.; Adamo, C.; Clifford, S.; Ochterski, J.; Petersson, G. A.; Ayala, P. Y.; Cui, Q.; Morokuma, K.; Malick, D. K.; Rabuck, A. D.; Raghavachari, K.; Foresman, J. B.; Cioslowski, J.; Ortiz, J. V.; Stefanov, B. B.; Liu, G.; Liashenko, A.; Piskorz, P.; Komaromi, I.; Gomperts, R.; Martin, R. L.; Fox, D. J.; Keith, T.; Al-Laham, M. A.; Peng, C. Y.; Nanayakkara, A.; Gonzalez, C.; Challacombe, M.; Gill, P. M. W.; Johnson, B.; Chen, W.; Wong, M. W.; Andres, J. L.; Gonzalez, C.; Head-Gordon, M.; Replogle, E. S.; Pople, J. A. *Gaussian 98*, A.6 ed.; Gaussian, Inc.: Pittsburgh, PA, 1998.
(26) Becke, A. D. *Phys. Rev. A* **1988**, *38*, 3098.
(27) Lee, C.; Yang, W.; Parr, R. G. *Phys. Rev. B* **1988**, *37*, 785.
(28) Ditchfield, R.; Hehre, W. J.; Pople, J. A. *J. Chem. Phys.* **1972**, *54*, 724.
(29) Verhoeven, J.; Dymanus, A.; Bluyssen, H. *J. Chem. Phys.* **1969**, *50*, 3330.
(30) Butler, L. G. The NMR Parameters for Oxygen-17. In *^{17}O NMR Spectroscopy in Organic Chemistry*; Boykin, D. W., Ed.; CRC Press: Boca Raton, 1991; p 325.
(31) Click, C. A.; Brow, R. K.; Cherry, B. R.; Alam, T. M. *J. Inorg. Phos. Chem. (Phos. Res. Bull.)* **2002**, *13*, 101−106.
(32) Brown, S. P.; Heyes, S. J.; Wimperis, S. *J. Magn. Reson. A* **1996**, *119*, 280.
(33) Gan, Z. *J. Am. Chem. Soc.* **2000**, *122*, 3242.
(34) Gan, Z. *J. Chem. Phys.* **2001**, *114*, 10845.
(35) Smith, M. E. *Bruker Rep.* **1990**, *1*, 33.
(36) Smith, M. E.; Taulelle, F.; Massiot, D. *Bruker Rep.* **1990**, *2*, 16.
(37) Clark, T. M.; Grandinetti, P. J. *J. Non-Cryst. Solids* **2000**, *265*, 75.
(38) Xue, X.; Kanzaki, M. *J. Phys. Chem. B* **2001**, *105*, 3422.
(39) Alam, T. M.; Segall, J. M. Manuscript in preparation.
(40) Schramm, S.; Oldfield, E. *J. Am. Ceram. Soc.* **1984**, *106*, 2502.
(41) Alam, T. M. *Int. J. Mol. Struct.* **2002**, *3*, 888.
(42) Xue, X.; Kanzaki, M. *Solid State Nucl. Magn. Reson.* **2000**, *16*, 245.
(43) Amoureux, J. P.; Fernandez, C. *Solid State Nucl. Magn. Reson.* **2000**, *16*, 339.
(44) Amoureux, J. P.; Fernandez, C. *Solid State Nucl. Magn. Reson.* **1998**, *10*, 211.
(45) Amoureux, J. P.; Pruski, M.; Lang, D. P.; Fernandez, C. *J. Magn. Reson.* **1998**, *131*, 170.
(46) Massiot, D.; Bessada, C.; Coutures, J. P.; Taulelle, F. *J. Magn. Reson.* **1990**, *90*, 231.
(47) Sternberg, U. *Solid State Nucl. Magn. Reson.* **1993**, *2*, 181.
(48) Grandinetti, P. J.; Baltisberger, J. H.; Farnan, I.; Stebbins, J. F.; Werner, U.; Pines, A. *J. Phys. Chem.* **1995**, *99*, 12341.
(49) Hoppe, U.; Walter, G.; Kranold, R.; Stachel, D. *Z. Naturforsch. A* **1998**, *53*, 93.
(50) Hoppe, U.; Walter, G.; Kranold, R.; Stachel, D. *J. Non-Cryst. Solids* **2000**, *263−264*, 29.